Morphologic properties derived from a simple cross-shore sediment transport model

N. G. Plant

Faculty of Technology and Management, University of Twente, Enschede, Netherlands

B. G. Ruessink[1] and K. M. Wijnberg

Institute for Marine and Atmospheric Research, Department of Physical Geography
Utrecht University, Utrecht, Netherlands

Abstract. This paper builds on the now classical discussions by *Bowen* [1980] and *Bailard* [1981] on the applicability and implications of *Bagnold*'s [1963] sediment transport model to nearshore profile modeling. We focus on the morphologic implications of both the strengths and weaknesses of Bagnold's model, isolating the transport terms that are well predicted (i.e., mean flow terms) from those that are not well predicted (i.e., transport due to correlations between flow and sediment load). We factor Bagnold's model into a dimensional transport magnitude and a nondimensional term. The nondimensional term describes the relative importance of transport due to undertow, gravity, and correlations between flow and sediment load. The transport magnitude largely determines the response time of nearshore profiles. For typical nearshore environments this response time was estimated to vary as a function of incident rms wave height (H_{rms}) from ~500 years ($H_{rms} \sim 0.5$ m) to 2 years ($H_{rms} \sim 3$ m). The relative importance of competing transport mechanisms is shown to depend strongly on the relative wave height (defined as the ratio of the rms wave height to the local depth). Simplified nearshore transport parameterizations that are a function of this variable were derived and were interrogated for the existence and form of equilibrium profiles. Several differences from previously computed equilibrium profiles were noted. First, because the relative wave height saturates in natural surf zones, equilibrium profiles converge to a relatively flat profile near the shoreline. Second, under some situations a seaward sloping equilibrium profile may not exist. Third, the long response times combined with unknown stability of an equilibrium profile make it difficult to assess the physical connection between theoretical equilibrium profiles and profiles observed in nature.

1. Introduction

At present, accurate prediction of nearshore bathymetric change at all relevant scales is impossible. Part of the difficulty is that the relevant scales span a very broad range, from millimeters (individual sand grains) to kilometers (the cross-shore width of the surfzone) and tens of kilometers (alongshore extent of littoral cells). The largest spatial scales are particularly important because they contain the majority of the spatial and temporal variability of nearshore bathymetric change [*Lippmann and Holman*, 1990; *Plant et al.*, 1999]. These are also the spatial and temporal scales that characterize human interactions with the coast. Unfortunately, the difficulty in modeling and prediction is acute at the largest scales, since evolution at this scale requires the integration over all smaller scales [*Roelvink and Brøker*, 1993].

Ideally, the interaction between the large-scale morphology (e.g., surf zone sandbars or the cross-shore profile as a whole) and small-scale processes (e.g., wave-driven hydrodynamics and sediment transport) can be described in terms of param-

eterizations of the small-scale processes. Examples of this sort of parameterization have been presented previously [*Bowen*, 1980; *Bailard*, 1981; *Stive*, 1986; *Roelvink and Stive*, 1989]. Accurate parameterizations of the small-scale processes allow predictions at the large scale to be based solely on calculations at the large scale. (An alternative approach might be to keep track of a large, but finite, number of sand and water particles in a modeling domain [*Werner and Fink*, 1993].)

The advantage of a purely large-scale model is its transparency, which allows direct quantification of the effects that various processes have on morphologic evolution. In particular, it enables the direct investigation of the mechanisms that allow existing bathymetry to influence its own evolution (i.e., morphologic feedback). One manifestation of this feedback is the potential for the bathymetry to be driven toward a steady state, or equilibrium. One of the goals of this paper is to broaden our understanding of how equilibrium states may be related to observed nearshore bathymetry, which is rarely, if ever, in equilibrium owing to constantly changing wave forcing.

Presently, it is not clear whether small-scale processes are understood well enough to derive parameterizations that can be used to accurately predict large-scale morphologic evolution. A widely accepted parameterization is *Bailard*'s [1981] adaptation of *Bagnold*'s [1963] sediment transport model. Several recent studies have compared this model to observed

---

[1]Now at WL/Delft Hydraulics, Delft, Netherlands.

bathymetric changes to predicted cross-shore profile evolution [*Thornton et al.*, 1996; *Gallagher et al.*, 1998]. These studies drove the sediment transport model with measured near-bed velocities, thus eliminating many hydrodynamic-related modeling errors. A primary conclusion from these studies was that onshore sediment transport was not well predicted, unless, locally, the mean flow was directed onshore [*Aagaard et al.*, 1998]. Predictions were more accurate during undertow-dominated conditions, where sediment transport was dominated by strong, seaward directed, near-bed, cross-shore mean flow. The failure to accurately predict onshore transport is particularly serious in the long term, since predicted onshore transport must somehow balance offshore transport in order to predict the existence of beaches. Because predictions of bathymetric change did not rely on a hydrodynamic model, a weakness in the adaptation of Bagnold's transport model was identified.

Bagnold's [1963] arguments may be physically reasonable, and they seem to capture some of the essential aspects of nearshore sediment transport, as indicated by its limited success in undertow-dominated conditions. There are not any clearly better alternatives to Bagnold's original, heuristically derived formulations [*Deigaard*, 1998]. (In fact, predictions made from other formulas, driven by measured velocities, have not been quantitatively compared to observed bathymetric changes.) The problem is that Bagnold's model yields specific, and thus rigid, parameterizations of some small-scale processes. Specifically, Bagnold sought to parameterize interactions associated with gravitational and near-bed turbulent forces that drive transport under unidirectional flow conditions. These are not the conditions that characterize the nearshore environment.

Contemporary theoretical and observational results provide very clear guidance toward those processes that are most relevant to cross-shore transport. These processes include wave-induced oscillatory flow, wave-driven mean flow (i.e., undertow and mean alongshore currents, which are tied to wave breaking), and wave-driven velocity skewness [*Roelvink and Stive*, 1989; *Black et al.*, 1995; *Thornton et al.*, 1996; *Gallagher et al.*, 1998; *Ruessink et al.*, 1998]. In light of these clearly significant variations from a unidirectional flow environment, it seems likely that *Bagnold*'s [1963] approach (i.e., one of parameterization), rather than his results (i.e., specific parameterizations), could lead us to improved prediction of nearshore transport and the ensuing bathymetric evolution. This is the approach that *Bailard* [1981] suggested would lead to improved prediction of large-scale patterns of sediment transport.

The intent of this paper is to add to the theoretical discussions of *Bowen* [1980], *Bailard* [1981], and others on the morphologic implications of *Bagnold*'s [1963] sediment transport model. Our discussion differs from previous process-based studies that have used Bagnold's model in that we do not investigate how the morphologic response is affected by adding or varying hydrodynamic parameterizations, which are often simply used to force the Bagnold transport model [e.g., *Roelvink and Stive*, 1989]. Instead, we investigate how variations in a simplified sediment transport parameterization, which is based on a fixed, small set of hydrodynamic processes, affect morphologic response. Another important difference between this and previous studies is our use of field observations of sediment transport to guide our empirical search for transport parameterizations. Because we will compute equilibrium profiles and use them to describe the morphologic implications of each transport formulation, we will not consider

parameterizations that specify morphologic response a priori, such as requiring an approach to a predetermined equilibrium profile [e.g., *Larson and Kraus*, 1995].

We take the following steps to achieve our goals. In section 2.1 we identify some very simple models of hydrodynamic processes associated with cross-shore–directed, wave-driven flow. Then, in section 2.2 we apply the hydrodynamic model to a generalized form of *Bagnold*'s [1963] bed load formula. The exercise yields transport associated with a mean flow and transport due to a sloping bed, consistent with previous work [e.g., *Bowen*, 1980; *Bailard*, 1981]. An additional term is added to this result in order to account for processes that drive onshore transport. This term would be the term associated with, for example, velocity skewness if Bagnold's formula were taken literally. In section 3 the assumptions made in the simple model are tested by comparing predictions to colocated velocity, pressure, and concentration measurements, which were obtained over a 6-week period on the Dutch coast. In section 4 we present a detailed discussion of the morphologic implications of the transport model. The model is used to predict equilibrium profiles, corresponding to constant offshore forcing conditions. We demonstrate the effect that several different transport parameterizations have on the equilibrium profile. Also in section 4 characteristic morphologic timescales associated with an approach to equilibrium are estimated. Finally in section 5 we summarize the conclusions drawn from the theoretical and observational results.

2. Theory
2.1. Simplified Hydrodynamics

Following the example of other cross-shore profile evolution models [*Bowen*, 1980; *Bailard*, 1981; *Stive*, 1986; *Roelvink and Stive*, 1989], we assume alongshore uniformity and that waves drive near-bottom, cross-shore flow. For simplicity (although not a necessity [see *Bailard*, 1981]), alongshore-directed flows are neglected. We consider two primary cross-shore flow components: the mean flow and fluctuations about the mean

$$U(x, t) = \bar{U}(x, t_m) + U'(x, t), \qquad (1)$$

where $\bar{U}$ is a time-mean velocity and U' is the fluctuating component. The "mean" of the flow is computed over a period that is long compared to the characteristic hydrodynamic timescale (e.g., that of a wave period) yet is short compared with a morphologic timescale. Therefore the so-called time-averaged quantities are allowed to vary slowly. The "slow" time variable, t_m, is related to the hydrodynamic time variable, t, via an as yet unspecified morphologic timescale, T_m, such that $t_m = t/T_m$. A prediction of the morphologic timescale will be a result of our model. Temporal changes in "time-averaged" quantities result from either slow morphologic changes or changes in the external forcing, which, for example, depends on the incident wave conditions.

Over the region relevant to sediment transport we assume that the flow is well approximated by vertically uniform flow. A reasonable model for the fluctuating velocity component is obtained from the shallow water approximation to linear wave theory [e.g., *Dean and Dalrymple*, 1984]

$$U'(x, t) = a(x, t_m) \sqrt{g/h(x, t_m)}$$

$$\cdot \{\sin [\theta(x, t_m) - \omega(t_m)t] + f_{nl}(x, t)\}, \qquad (2)$$

where a is the local amplitude of a monochromatic wave train, g is the acceleration of gravity, ω is the wave frequency (radi-
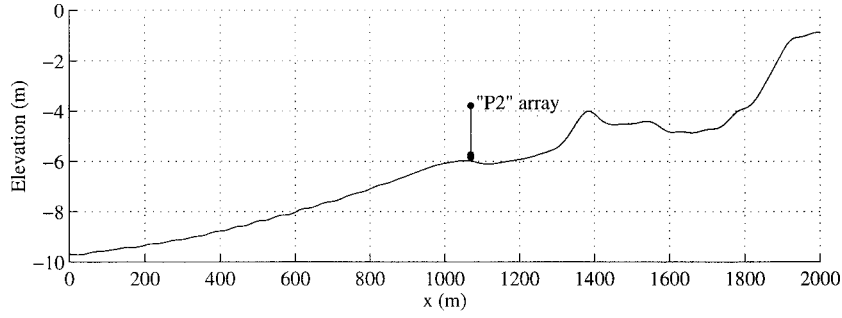
Figure 1. Cross-shore profile at Terschelling, sampled in October 1995. Elevations are referenced to the Dutch mean sea level datum Normaal Amsterdams Peil (NEP). Instruments at location "P2" are marked with dots at 2.2 m above the bed (pressure gage), 0.25 m (EMF), and 0.15 m (OBS).

ans), θ is the spatial phase shift associated with wave propagation, and h is the local still water depth. The function f_{nl} describes velocity fluctuations due to wave nonlinearity, which we will not consider in detail. Hereinafter, all variables that are not explicitly identified as constants or are not explicitly functions of the fast time, t, are implicitly functions of the morphologic time variable, t_m, and cross-shore position, x.

We assume that an offshore-directed mean flow (i.e., undertow) balances the onshore-directed mass flux of water above trough level. A simple expression for this mass flux, M ($\mathrm{m}^3\,\mathrm{m}^{-1}$ s^{-1}), has been derived from linear wave theory [*Phillips*, 1977]:

$$M = \rho a^2 \sqrt{g/h}. \tag{3}$$

If we assume depth uniform flow below the still water level, then

$$\bar{U} = -\frac{M}{(\rho h)} = -\frac{a^2}{h}\sqrt{\frac{g}{h}}, \tag{4}$$

where we use a sign convention with the positive direction pointing onshore (see Figure 1). Equation (4) is a simplified form of many existing undertow models, which have been shown to be reasonably accurate [*Masselink and Black*, 1995]. More complicated forms include, for example, stronger sensitivity to wave breaking and a more detailed description of the vertical structure of the mean flow [*Stive and Wind*, 1986; *Haines and Sallenger*, 1994; *Stive and de Vriend*, 1994].

Linear wave theory can be applied to the random wave heights (or amplitudes) that are observed in nature in order to derive a statistical description of the flow. Given a narrowband random wave spectrum, wave amplitudes are Rayleigh distributed [*Cartwright and Longuet-Higgins*, 1956] and have a probability distribution function (pdf) given by $p(a) = (a/\sigma^2)\exp[-0.5(a^2/\sigma^2)]$, where σ^2 is the sea surface variance. Corresponding sea surface elevations and wave-driven velocities are Gaussian distributed. The velocity variance, σ_u^2, is given by

$$\sigma_u^2 = \sigma^2 \frac{g}{h} \tag{5a}$$

or

$$\sigma_u^2 = \frac{H_{\mathrm{rms}}^2}{8}\frac{g}{h}, \tag{5b}$$

where H_{rms} is the root-mean-square wave height ($H_{\mathrm{rms}} = 2\sqrt{2}\sigma$). We neglect, for now, the contribution of the nonlinear term in (2).

The expected value of a^2 (i.e., integral of $a^2 p(a)\,da$ over all values of a is $2\sigma^2$. Thus the expected value of the mean flow due to random waves is (from (4))

$$\bar{U} = -2\frac{\sigma^2}{h}\sqrt{\frac{g}{h}} \tag{6a}$$

or

$$\bar{U} = -\frac{y}{\sqrt{2}}\sigma_u, \tag{6b}$$

where the second form is in terms of the so-called relative wave height [*Ruessink et al.*, 1998], which we define as

$$y = H_{\mathrm{rms}}/h. \tag{7}$$

The relative wave height will play an important role in the following development of a sediment transport formulation.

2.2. Sediment Transport

The local, depth-integrated and time-averaged sediment transport rate is obtained from the time-averaged product of the depth-uniform velocity, U, and the sediment load, S:

$$\bar{Q} = \bar{S}\bar{U} + \overline{S'U'}. \tag{8}$$

Again, the time average (indicated by overbars) is taken over a period that is short compared to the morphologic timescale. The sediment load, S, is the depth-integrated mass of sediment per horizontal square meter:

$$S = \int_z C(z)\,dz, \tag{9}$$

where C is the sediment-mass concentration (kg sediment)/(m^3 water column).

It is natural to decompose the transport into a mean and fluctuating component. Not only does this help to illustrate the contribution of various processes to the total transport, but it makes a clear division between the terms that *Bagnold*'s [1963] original flow model considered (i.e., mean flow component) and those that have been shown to be poorly modeled (i.e., onshore transport associated with velocity fluctuations). The second term in (8) is, by definition, the cross covariance between the sediment load and the velocity, which can be redefined as

$$\overline{S'U'} \equiv R_{su}\sigma_s\sigma_u. \tag{10}$$

Here R_{su} is the cross correlation (which is nondimensional) between U and S, and σ_s is the standard deviation of the sediment load.

Because the sediment load is a positive quantity, its mean and standard deviation are likely related to each other. This relationship depends on the pdf of sediment load values. For example, if a Rayleigh distribution is a good model for the sediment load pdf, then $\sigma_s \approx 0.5\bar{S}$. We will assume that $\sigma_s = c_1\bar{S}$, where c_1 is a constant of $O(1)$. (The parameter c_1 may be a function of sediment properties.) By substituting this "trick" into (10), the result, along with the mean flow prediction of (6) into (8), yields

$$\bar{Q} = \sigma_u \bar{S}\left\{-\frac{y}{\sqrt{2}} + c_1 R_{su}\right\}. \tag{11}$$

The term outside of the braces in (11) scales the potential magnitude of transport, and it may be thought of as a sediment "stirring" term. The nondimensional terms inside the braces control, primarily, the direction of transport, describing the balance between several competing transport mechanisms.

Given an arbitrary depth profile and offshore wave statistics, a simple wave transformation model [e.g., *Thornton and Guza*, 1983] can be used to predict the rms wave height over the entire profile. Thus it is possible to predict the values of σ_u (via (5)) and y (via (7)). Closure of the present transport model requires a description of the time-averaged sediment load, $\bar{S}$, and correlation term, R_{su}, in terms of the local depth and wave height alone.

2.2.1. Bed load formula. We use *Bagnold*'s [1963] heuristic arguments to derive an expression for the mean sediment load. We require, at this point, only a dimensionally correct form and do not formally distinguish bed load from suspended load transport. For simplicity, we consider Bagnold's bed load formulation alone.

Bagnold [1963] assumed that the mean normal stress exerted by the weight of the bed load is supported, on average, by the mean tangential stress. The tangential stress is the applied bed shear stress from the fluid flow, τ, plus the downslope contribution of gravity. Bagnold hypothesized that the ratio of the tangential to normal forces was equal to the tangent of the angle of repose, ϕ:

$$\left|Sg \sin\beta + \tau\frac{(\rho_s - \rho)}{\rho_s}\right| = Sg \cos\beta \tan\phi, \tag{12}$$

where S is the sediment load defined in (9), ρ_s is the sediment density, and β is the beach slope, which is negative for a seaward slope. This slope definition describes the depth gradient, such that $\tan\beta = \partial h/\partial x$.

An explicit expression for the sediment load is obtained if the magnitude of the fluid shear stress term always exceeds the magnitude of the downslope gravitational term. For simplicity, we assume that the bed slope is much smaller than the angle of repose. These assumptions are the same as those of *Bowen* [1980] and *Bailard and Inman* [1981]. The result is

$$S = \frac{(\rho_s - \rho)}{\rho_s g}\frac{|\tau|}{\tan\phi}\left\{1 + \frac{|\tau|\tan\beta}{\tau\tan\phi}\right\}. \tag{13}$$

Equation (13) describes a relationship between statistically averaged values of shear stress and sediment load. *Bagnold*'s [1963] original formulation intended to characterize a unidirectional flow situation in which only turbulent fluctuations

were considered. We wish to apply this formula to the nearshore environment, where the wave-driven shear stress fluctuations are large. For the moment, we adopt the approach employed by *Bowen* [1980] and *Bailard and Inman* [1981] and assume that the sediment load is in equilibrium with the shear stress over all wave phases.

2.2.2. Time-averaged sediment load. We assume that the shear stress is the only quantity in (13) that varies over the averaging time needed to compute the mean sediment load. *Bagnold* [1963] and others assumed that the appropriate stress could be related to the velocity using a drag relationship:

$$\tau = C_f'\rho U|U|. \tag{14a}$$

Here C_f' is a modified friction coefficient that acknowledges Bagnold's transport efficiency factor, ε, such that $C_f' = \varepsilon C_f$ (i.e., C_f is $O(10^{-3})$ and ε is $O(10^{-2} - 10^{-1})$ [*Gallagher et al.*, 1998]). The time-averaged sediment load can be computed from (13) and (14a) by integrating over the Gaussian velocity pdf. The integral must be split into positive and negative shear stress contributions, since $|\tau| = \tau$ if $\tau \geq 0$ and $|\tau| = -\tau$ otherwise. These integrated quantities are

$$|\bar{\tau}|^+ = \frac{\rho C_f'\sigma_u^2}{2}\{(1 + \chi^2)[1 + \mathrm{erf}(\chi\sqrt{2})]$$
$$+ (\sqrt{2/\pi})\chi\exp(-\chi^2/2)\} \tag{14b}$$

$$|\bar{\tau}|^- = \frac{\rho C_f'\sigma_u^2}{2}\{(1 + \chi^2)[1 - \mathrm{erf}(\chi\sqrt{2})]$$
$$- (\sqrt{2/\pi})\chi\exp(-\chi^2/2)\}, \tag{14c}$$

where $|\bar{\tau}|^+$, $|\bar{\tau}|^-$ correspond to the contributions from the positive (onshore) and negative (offshore) shear stresses, respectively; χ is the ratio of the mean to standard deviation of the velocity,

$$\chi = \bar{U}/\sigma_u \tag{15a}$$

or

$$\chi = -y/\sqrt{2}, \tag{15b}$$

where the second form uses the result of (6). The error function, erf(χ), and the exponential term weight the relative contribution of the positive and negative shear stress contributions to the mean shear stress.

Inserting (14b) and (14c) (in terms of the relative wave height) into (13) yields

$$\bar{S} = c_2\frac{\rho}{g}\frac{\sigma_u^2}{\tan\phi}\left\{\left(1 + \frac{y^2}{2}\right)\right.$$
$$\left. - \frac{\tan\beta}{\tan\phi}\left[\left(1 + \frac{y^2}{2}\right)\mathrm{erf}\left(\frac{y}{2}\right) + \frac{y}{\sqrt{\pi}}\exp\left(-\frac{y^2}{4}\right)\right]\right\},$$
$$\tag{16a}$$

where $c_2 \equiv C_f'(\rho_s - \rho)/\rho_s$. Equation (16a) shows that the wave velocity variance contributes to a sediment stirring term. The stirring may be enhanced by the addition of a mean flow, as is represented by the first occurrence of the term $[1 + (y^2/2)]$. Additionally, a mean current in the downslope direction enhances the sediment load. The dependence on the relative wave height is similar to the results of *Bailard* [1981], *Stive*

[1986], and *Wright et al.* [1991], which also isolated the normalized mean flow term, χ.

Equation (16a) can be simplified further for the case where both the relative wave height and slope are small. Field measurements have shown that the relative wave height, y, saturates because of wave breaking at values ranging from 0.25 to ~0.4 [*Thornton and Guza*, 1982; *Sallenger and Holman*, 1985; *Raubenheimer et al.*, 1996]. Beach slopes are often in the range of $O(0.01)$ to $O(0.1)$. As a result, for many physically reasonable situations we can neglect the terms of $O(y^2)$ and $O(y \tan \beta / \tan \phi)$ in (16a) to get

$$\bar{S} = c_2 \frac{\rho}{g} \frac{\sigma_u^2}{\tan \phi}. \tag{16b}$$

We evaluated (16a) and (16b) and found that (16b) underestimates (16a) by 10% for extreme conditions of $y = 0.5$ and $\tan \beta / \tan \phi = 0.2$.

The underlying sediment load model (equation (13)), shear stress model (equation (14a)), and Gaussian velocity distribution can be used to get higher-order statistics as well, such as the variance of the sediment load:

$$\sigma_s^2 \approx 2 \left\{ c_2 \frac{\rho}{g} \frac{\sigma_u^2}{\tan \phi} \right\}^2 \left\{ 1 - 6 \frac{y}{\sqrt{\pi}} \frac{\tan \beta}{\tan \phi} + y^2 \right.$$
$$\left. + O \left(\frac{\tan \beta}{\tan \phi} y^3, \frac{\tan^2 \beta}{\tan^2 \phi} y^2 \right) \right\}. \tag{17}$$

This result predicts that the ratio of the standard deviation to the mean of the sediment load (i.e., c_1) is $O(1)$. Likewise, the predicted correlation between the sediment load and velocity fluctuations is (to first order in slope and relative wave height)

$$R_{su}^{\text{Gaussian}} \approx \left(\frac{2}{\sqrt{\pi}} \frac{\tan \beta}{\tan \phi} - y \right). \tag{18a}$$

The "Gaussian" superscript indicates that this result is for purely Gaussian velocity distributions (and total faith in equation (13)), which drive downslope and downcurrent transport.

Presumably, there is at least one more term that accounts for the effect of other wave and sediment transport processes (such as wave nonlinearity, threshold of grain motion, effect of ripples). In particular, we are missing any term that will account for onshore transport in the presence of an offshore sloping bed. This heuristic argument suggests that we substitute into (11) a correlation term with the form

$$R_{su} \approx R_{su}^{\text{Gaussian}} + R_{su}^{\text{other}}. \tag{18b}$$

For example, if the "other" contribution results from the velocity skewness, then it is straightforward (through (13)) to show that, to first order in skewness,

$$R_{su}^{\text{other}} \approx \psi / \sqrt{2}, \tag{18c}$$

where $\psi = \overline{(U - \bar{U})^3} / \sigma_u^3$ is the normalized velocity skewness [*Elgar and Guza*, 1985; *Doering and Bowen*, 1995]. We suspect that the skewness dependence in (18c) is a weak point in the adaptation of *Bagnold*'s [1963] model to the nearshore, since this is the term that drives onshore transport, which was shown to be poorly predicted [*Thornton et al.*, 1996; *Gallagher et al.*, 1998]. At this point, it is not necessary to interpret the skewness term (or any of the transport terms) too literally. The general form of the transport equation is of primary interest.

2.2.3. Time-averaged sediment transport model. Inserting the approximate, mean sediment load (equation (16b)) and the partially specified form of the correlation term (equations (18a) and (18b)) into the mean transport equation (equation (11)) yields

$$\bar{Q} = c_2 \frac{1}{16\sqrt{2}} \frac{\rho \sqrt{g}}{\tan \phi} H_{\text{rms}}^3 h^{-3/2} \left\{ - \left(\frac{1 + c_1 \sqrt{2}}{\sqrt{2}} \right) y \right.$$
$$\left. + c_1 \left(\frac{2}{\sqrt{\pi}} \frac{\tan \beta}{\tan \phi} + R_{su}^{\text{other}} \right) \right\}, \tag{19}$$

where we have inserted the velocity variance prediction of (5) in terms of the rms wave height. Equation (19) exposes some properties that are shared by most transport formulae and are directly relevant to nearshore morphologic evolution. First, the potential magnitude of transport (those terms outside of the braces, which are always positive in sign) scales with the cube of the rms wave height. An increase in the local wave height leads to a nonlinear increase in the transport and, potentially, the rate of morphologic response. Second, the magnitude of transport decreases nonlinearly with increasing water depth. This is consistent with the longer response time of outer sandbars (T_m of several years), compared to inner sandbars (T_m less than a year), which were quantified from bathymetric surveys at Duck, North Carolina [*Plant et al.*, 1999].

Finally, the relative importance of slope, undertow, and sediment-flow correlation determines the direction (onshore or offshore) of transport. Before we can investigate the role that this balance plays in morphologic evolution, we must specify the form of the correlation term, R_{su}^{other}. As an alternative to continued theoretical development, we choose to extract a suitable empirical formulation for this term from an analysis of field data. We will use the theory developed so far to guide our use of empiricism.

3. Comparison to Field Observations of Small-Scale Processes

Some very specific (though not necessarily restrictive) assumptions were made in order to derive the present sediment transport model. Using sample statistics estimated from field observations, we can evaluate the accuracy of some of our assumptions. Colocated velocity, pressure, and concentration measurements were collected as part of the Nourtec experiment (October–November 1995) on the coast of the Dutch island of Terschelling. We utilized observations from a single location in ~6 m depth, near the crest of a shore-parallel sandbar (Figure 1), corresponding to campaign T4 and location P2 in the analysis by *Ruessink et al.* [1998] (hereinafter referred to as R1998). Velocity measurements were obtained from an electromagnetic flow meter (EMF), which was situated ~25 cm from the bed. Concentrations were measured with an optical backscatter sensor (OBS) situated ~15 cm from the bed. The pressure sensor, used to estimate the sea surface elevation, was situated ~2.2 m from the bed. The observations spanned a 6-week period and consisted of a total of 707 individual 34-min bursts, each sampled at 2 Hz. One burst was sampled each hour. These data have been extensively analyzed by R1998, and we refer to their paper for more detailed explanations.

From each burst we estimated the means and variances of sea surface elevation, cross-shore velocity, and sediment con-
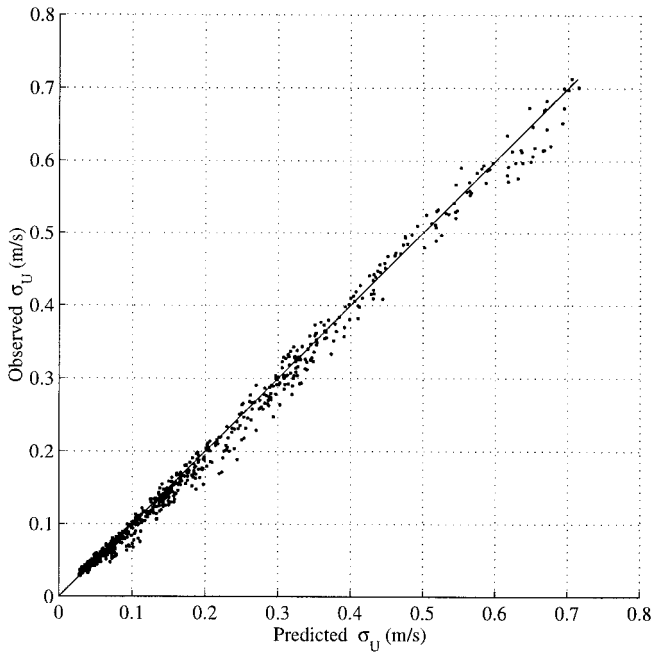
Figure 2. Cross-shore velocity standard deviation (σ_u) calculated from velocity observations 25 cm above bed. Velocity standard deviation estimates (dots) are plotted against linear wave theory prediction based on sea surface variance estimate. Solid line is line of perfect agreement with theory.

centration. Additionally, we estimated the correlation between velocity and sediment concentration fluctuations, and we estimated the velocity skewness. All of the variance-based statistics were calculated from the wind wave and infragravity frequency range as defined by R1998 ($f > 0.004$ Hz). The pressure signal was not corrected for short wave attenuation, and no attempt was made to account for oblique angles of wave approach or for the effect of alongshore currents.

3.1. Velocity Terms

Figure 2 shows that the predicted velocity variance (estimated via equation (5)) agreed well with the observed cross-shore velocity variance ($R^2 = 0.99$), clearly indicating the applicability of the shallow water approximation to linear wave theory. Next, Figure 3 shows the relationship between predicted and observed mean velocities. A significant linear correlation was found ($R^2 = 0.68$), but the observed velocities were, on

average, nearly twice as large as the prediction of (6). It appears that the observed mean velocities increased nonlinearly as the predicted value increased, since the deviations from the model were largest (but negative) at high mean flow speeds. Finally, the velocity skewness, which is a relevant variable in both *Bowen*'s [1980] and *Bailard*'s [1981] transport equations, is shown in Figure 4. Skewness increased nonlinearly, but monotonically, as both the Ursell number ($Ur = g(a/h)(\omega^2 h)^{-1}$) and the relative wave height increased. The Ursell number provides a characterization of wave nonlinearity and is potentially useful for predicting wave velocity skewness [*Doering and Bowen*, 1995].

3.2. Sediment Load Terms

The assumption that the mean and standard deviation of the sediment load are proportional to each other is addressed qualitatively by examining the relationship between mean and standard deviation of the concentration time series. Figure 5a shows a significant linear correlation ($R^2 = 0.80$), with a slope of nearly 1. The obvious presence of two populations of the data displayed in Figure 5a deserves some explanation. One population exhibits a steep increase in concentration standard deviation with increasing mean concentration (slope of ~1). The other population is associated with a gentler slope of ~0.5. Figure 5b shows that these populations were separated into two relative wave height regimes. The transition region between slopes of ~0.5 and slopes of ~1 occurred within the range $y = 0.1$ to 0.15.

The existence of these populations may be a result of actual sediment transport mechanics or it may be an artifact of the sampling method. A change in transport mechanics may result from a transition in the bed state. R1998 cited a prediction for a transition from a rippled bed to a plane bed when the characteristic near-bed velocity (i.e., $\sqrt{2}\sigma_u$) exceeded 0.8 m s^{-1}, which corresponded to a relative wave height of ~0.2 (this value results from an empirical relationship, $\sigma_u = 2.8y$ m s^{-1}, $R^2 = 0.98$, that was fit to the present data). Alternatively, a transition from bed load to suspended load dominance is expected when the ratio of the near-bed velocity to the fall velocity exceeds, roughly, 10 [*Bowen*, 1980]. The fall velocity at the field site was ~0.02 m s^{-1}, suggesting well-developed suspension for $y > 0.05$. The onset of suspension seems to be the most likely physical explanation for the variation in sediment statistics.

A potentially important sampling bias can be seen in a comparison of the estimated concentration variance to the estimated (from EMF observations) velocity variance. Figure 6
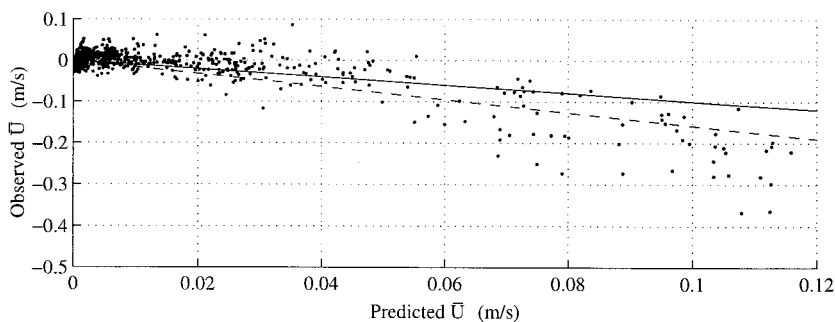
Figure 3. Cross-shore mean velocity ($\bar{U}$) calculated from velocities observed 25 cm above bed. Mean velocity estimates (dots) are plotted against linear theory prediction. Solid line is line of perfect agreement with theory. Dashed line is best linear relationship (slope was -1.6, $R^2 = 0.68$).
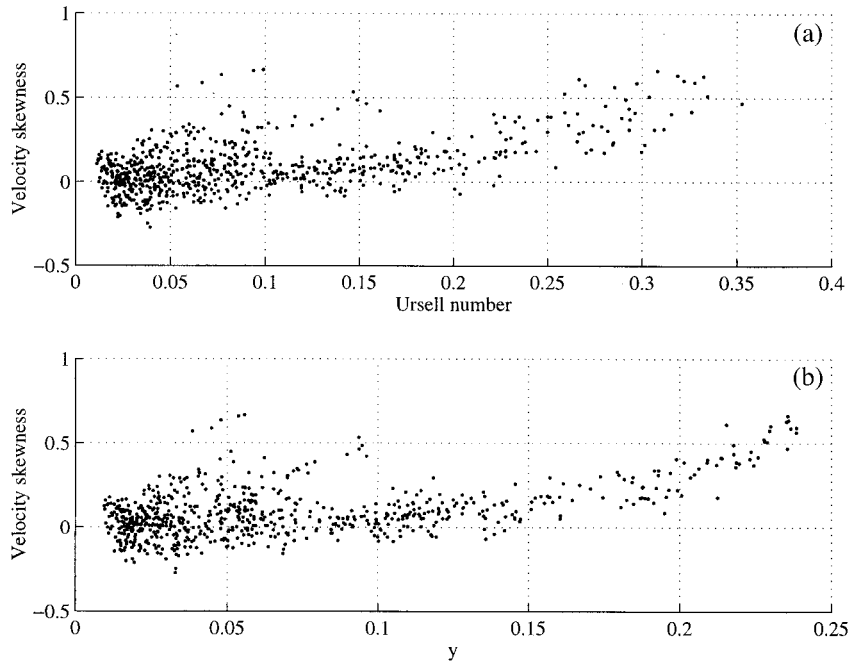
Figure 4. Cross-shore velocity skewness calculated from velocity observations 25 cm above bed. Skewness estimates are plotted against (a) Ursell number (in shallow water $Ur = g[H_{rms}/\sqrt{8}h)(\omega^2 h)^{-1}]$ and (b) relative wave height ($y = H_{rms}/h$).
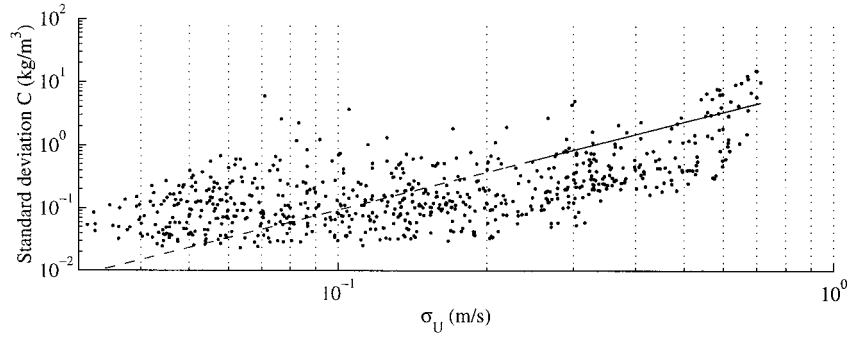
shows that the concentration standard deviation was approximately constant at velocity standard deviations lower than ~ 0.2 m s^{-1}. This indicates a noise floor (perhaps corresponding to little or no observable suspension) and hinders our ability to interpret data in this region (i.e., $y < 0.1$).

3.3. Correlation Terms

Equations (18a)–(18b) suggest that the sediment-flow correlation may be solely a function of the relative wave height and the local slope, having a general form of
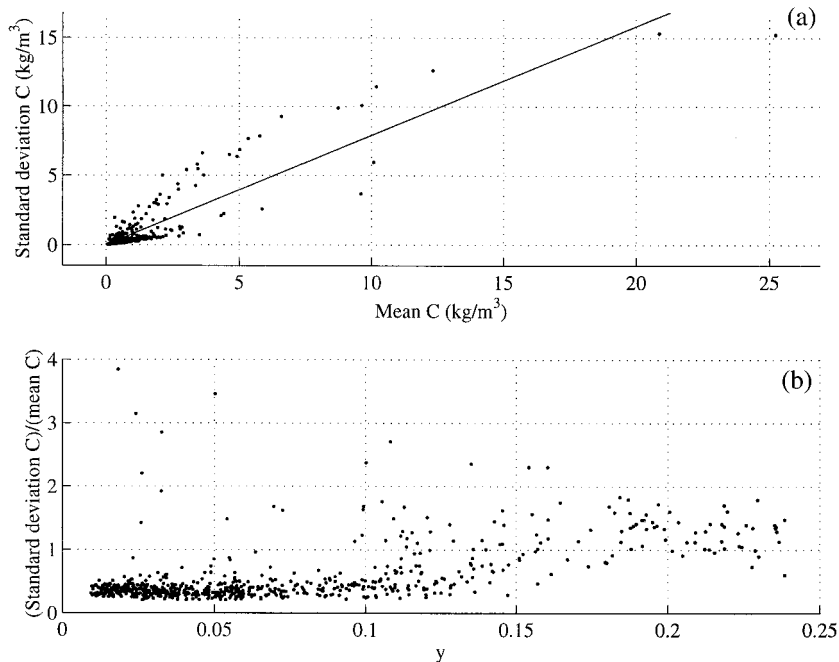
Figure 5. (a) Concentration standard deviations (dots) plotted against corresponding mean concentrations. Sample means and variances were estimated from OBS observations 15 cm above bed. Solid line shows the best fit linear relationship passing through the origin. (b) The two populations of the ratio of the standard deviation to the mean concentration appeared at different relative wave heights, y. The transition between regions begins at about $y = 0.1$, where typical velocity standard deviations were 0.3 m s^{-1}.
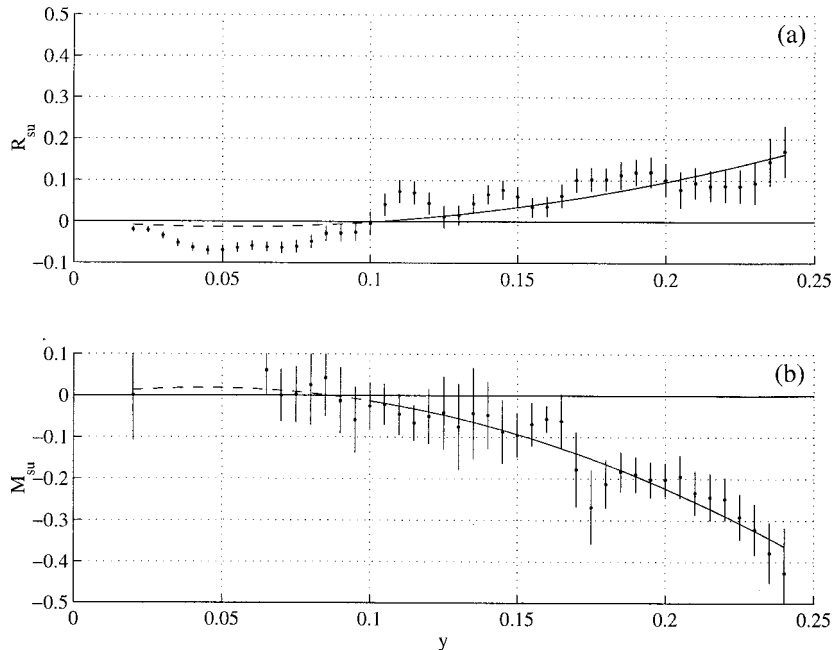
Figure 6. Concentration standard deviation calculated from OBS observations 15 cm above bed. Estimates (dots) are plotted against the velocity standard deviation. Solid line shows the best fit ($R^2 = 0.44$) linear relationship to the square of the velocity standard deviation (i.e., the relationship predicted by the linearized version of equation (17)). The dashed portion of the line corresponds to $y < 0.1$, and these data were not used in the regression.

$$R_{su} = \{r_0 \tan \beta + r_1 y\} + F(y), \qquad (20)$$

where r_0, and r_1 are constants (potentially functions of sediment characteristics). The terms in braces in (20) describe the contribution from the Gaussian model (equation (18a)). The function $F(y)$ accounts for the contribution by R_{su}^{other} (equation (18b)). The key argument here, which is suggested by both the theoretical results and observational data, is that R_{su} is a function of the local beach slope and a single forcing variable, y. This point can be argued equally well via the presumed skewness relevance [Bowen, 1980; Bailard, 1981] and the relationship between skewness and y that is shown in Figure 4a.

Estimates of the correlation between the fluctuating components of concentration and velocity are shown in Figure 7a, plotted against the relative wave height. For values of the relative wave height below ~0.1 the correlations were clearly negative (i.e., significantly nonzero after averaging over subregions of y, each having width of 0.02), indicating offshore transport. We do not expect a transport contribution from the symmetric velocity fluctuations occurring in a hydrodynamic regime characterized by Gaussian velocity distributions (Figures 4b and 8). Equation (18a) (which describes the contribution due to symmetric oscillatory currents superimposed on a small mean flow over a gently sloping bed) clearly points out that because the transport is a nonlinear function of velocity, a

Figure 7. (a) Estimates of normalized transport contributions due to correlations between concentration and velocity fluctuations and (b) contributions due to mean concentrations and velocities ($M_{su} = \{\bar{U}/\sigma_u\}\{[\text{mean } C]/[\text{standard deviation } C]\}$). Estimates are from velocity observations 25 cm above bed and concentration observations 15 cm above bed. Dots indicate mean values estimated over equally spaced ranges of the relative wave height, y. Error bars represent 95% confidence intervals about the means. Solid lines illustrate the parameterizations $R_{su} = r_1 y + r_2 y^2$ and $M_{su} = m_1 y + m_2 y^2$, which were fit to the data via linear regression ($r_1 = -0.5$, $r_2 = 5.0$, $R^2 = 0.76$, and $m_1 = 0.9$, $m_2 = -9.9$, $R^2 = 0.96$). Dashed lines show region where data were omitted from the regression analysis.
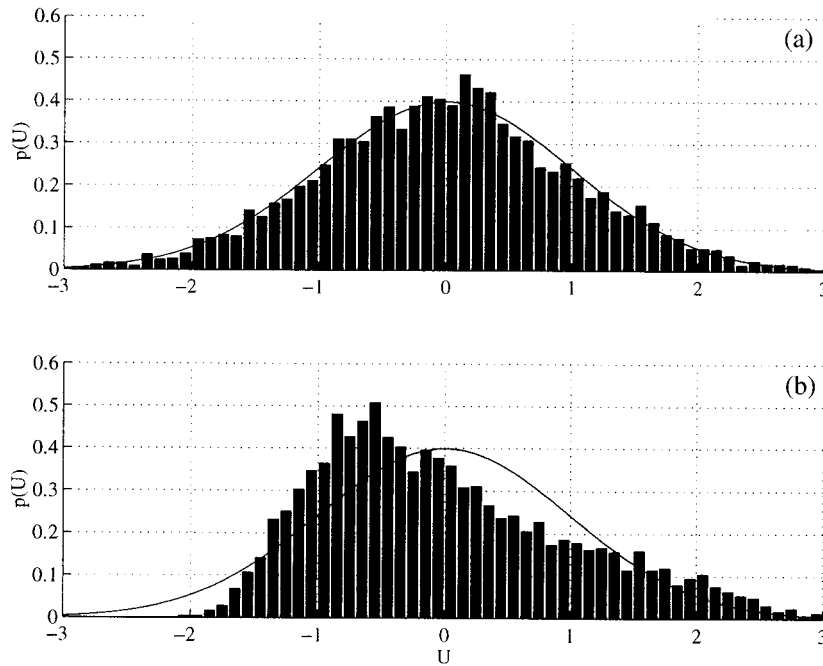
Figure 8. Normalized cross-shore velocity pdf's (i.e., zero mean, unit variance). The two cases represent (a) nearly Gaussian velocity pdf under low relative wave height conditions (hour 247, $y = 0.14$, $\bar{U} = -0.04$ m s^{-1}, $\sigma_u = 0.41$ m s^{-1}, skewness $= 0.13$) and (b) significantly skewed pdf under high relative wave height conditions (hour 579, $y = 0.24$, $\bar{U} = -0.34$ m s^{-1}, $\sigma_u = 0.63$ m s^{-1}, skewness $= 0.67$). Curves show Gaussian pdf, and bars show estimated pdf's.

small mean flow or small slope will "leak" an offshore transport component into the correlation term. A slope contribution is unlikely because the sensors were located near the bar crest (which moved very little over the study period). The mean velocity measurements are unreliable in the low relative wave height regime, so, in spite of its statistical robustness and potential consistency with theory, the offshore transport due to flow-concentration correlation is difficult to interpret.

At high values of y the correlation estimates were generally positive (driving onshore transport). The general model (equation (20)) with $F(y) = r_1 y + r_2 y^2$ was fit to the data in the range $y > 0.1$. We arbitrarily chose $r_0 = 0$, since the low-y region of the model was not constrained by data. The skill of this model was significant ($R^2 = 0.76$). This suggests that a polynomial function of relative wave height may be a generally appropriate parameterization to use in the transport formulation.

3.4. Mean Flow and Sediment Load Term

The contribution from the mean flow to the term in braces in (19) is a linear function of the relative wave height. Figure 7b shows estimates of this term, plotted against the relative wave height. This estimate increases nonlinearly with increasing relative wave height, consistent with the observed nonlinear increase in the undertow and, presumably, the nonlinear increase in the sediment load. A more reasonable parameterization for the mean flow contribution is a polynomial as before (equation (20)), but with $F(y) = m_1 y + m_2 y^2$, constrained to pass through zero at $y = 0$). This model was fit to the observed mean flow contribution (applied to the region $y > 0.1$), and it represented the data well ($R^2 = 0.96$).

4. Discussion: Morphologic Implications

4.1. Generalized Transport Equation

The theoretical development presented so far suggests that, in general, a reasonable parameterization of cross-shore sediment transport consists of a magnitude term multiplied by a term that describes the relative importance of sediment transport due to mean flow, slope, and flow-sediment correlation:

$$\bar{Q}(x, t_m) = q(x, t_m) r(x, t_m), \qquad (21a)$$

where $q(x, t_m)$ represents the magnitude (e.g., term outside braces in (19)) and $r(x, t_m)$ represents the relative importance of competing transport mechanisms (e.g., term inside braces in (19)). This form of transport model has been suggested by others [*Horikawa*, 1981]. The magnitude term describes, essentially, the stirring of sediment, which, for simplicity, we have assumed to be dominated by the wave-driven velocity variance, leading to

$$q = c_2 \frac{1}{16\sqrt{2}} \frac{\rho\sqrt{g}}{\tan\phi} H_{\mathrm{rms}}^3 h^{-3/2}. \qquad (21b)$$

The relative importance term, $r(x, t_m)$, accounts for transport due to the mean flow and the flow-sediment correlations. Both the simplified transport theory and the transport observations (i.e., Figure 7) indicated that the relative importance of several competing transport mechanisms depends, in part, on the relative wave height and the local slope, and this dependence may be captured in the form of a polynomial expression, such as

$$r(\tan\beta, y) = r_0 \tan\beta + r_1 (y/y_c)^p [1 - y/y_c], \qquad (21c)$$
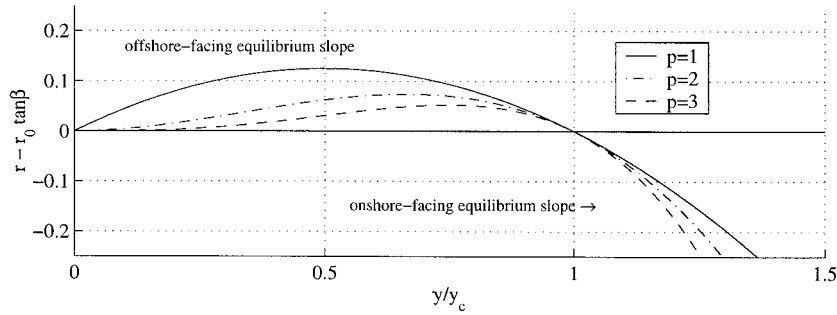
Figure 9. Nondimensional transport parameterization, r (equation (21c)) as a function of the relative wave height, y. The function is plotted for several polynomial orders, p (values of other parameters were $r_0 = 2.25$, $r_1 = 0.5$, $y_c = 0.3$). Since $r = 0$ for equilibrium, the equilibrium slope can be inferred from the abscissa values. Assuming that r_0 is positive, a clear prediction is an onshore-facing equilibrium slope at large relative wave heights.

where r_0, r_1, y_c, and p are constant parameters, while $\tan \beta$ and y are variables. Setting $p = 0$ yields

$$r(\tan \beta, y) = r_0 \tan \beta(x) + r_1 - r_1 y/y_c, \qquad (21d)$$

which can be used to recover the term in braces in (19) if $r_0 = 2c_1/(\tan \phi \sqrt{\pi})$, $r_1 = c_1 R_{su}^{\text{other}} = \text{const}$, and $r_1/y_c = (1 + c_1 \sqrt{2})/\sqrt{2}$. Setting $p = 1$ would give a quadratic formulation that is consistent with the results from the field data analyses shown in Figure 7.

The form of r for several choices of $p > 0$ is shown in Figure 9. Figure 9 shows only the relative wave height dependence, as the linear slope dependence has been removed. We use values of $r_0 = 2.25$, $r_1 = 0.5$, and $y_c = 0.3$. At low values of y the mean flow and correlation mechanisms vanish (as does the potential to transport sand grains). The initial dominance of onshore transporting mechanisms, which is an essential feature of this parameterization, reaches a maximum at $y/y_c = p/(p + 1)$. The value of r_1 scales the magnitude of this maximum. Neglecting the slope contribution, the onshore and offshore transporting mechanisms balance at $y = y_c$. Finally, at large y/y_c, offshore transport dominates. Presumably, y_c scales with the maximum "saturated" value of H_{rms}/h, since this provides a parameterization of breaking intensity, as already mentioned. If the model given by (21c) is to be quantitatively accurate, y_c may not be a constant, since the saturation value of y varies with slope, depth, and wave period [*Sallenger and Holman*, 1985; *Raubenheimer et al.*, 1996]. We will not pursue this complication.

4.2. Equilibrium

Because beach slope is included in the transport formulae (equations (19) and (21a)–(21c)), there is the potential for the slope term to balance the other transport terms, resulting in zero net transport at a point. If the transport vanishes everywhere, then an alongshore-uniform profile is at a state of morphologic equilibrium, since the gradients in transport, which drive profile change, also vanish. We can interrogate the originally derived transport formulation (equation (19)) and the generalized form (equations (21a)–(21c)) to determine conditions that allow morphologic equilibrium, and we can determine the equilibrium profile shapes that are consistent with these equations.

In (19) a condition of equilibrium requires the term in braces to vanish, and

$$0 = \tan \beta(x) + \frac{\sqrt{\pi}}{2} \tan \phi \left\{ -\left(1 + \frac{1}{c_1 \sqrt{2}} \right) y(x) + R_{su}^{\text{other}}(x) \right\}. \qquad (22a)$$

Several conditions may lead to equilibrium, including the following: (1) correlation term balances seaward sloping bed, (2) correlation term balances undertow, and (3) undertow balances landward slope. In deep water the relative wave height can be neglected. If we assume for illustrative purposes that the sediment-flow correlation term is constant (i.e., $R_{su}^{\text{other}} = R_{su}^{\text{const}}$), then the slope is also constant:

$$\tan \beta(x) = -\frac{\sqrt{\pi}}{2} \tan \phi R_{su}^{\text{const}}. \qquad (22b)$$

From Figure 7a, a reasonable estimate of the correlation term is 0.1 and $\tan \phi$ is ~ 0.5, leading to a predicted beach slope of $O(1{:}20)$.

Alternatively, in shallow water the relative wave height approaches a constant (e.g., for the present data set $y \rightarrow 0.25$) and

$$\tan \beta(x) = \frac{\sqrt{\pi}}{2} \tan \phi \left\{ \left(1 + \frac{1}{c_1 \sqrt{2}} \right) 0.25 - R_{su}^{\text{const}} \right\}. \qquad (22c)$$

An equilibrium profile with a seaward (negative) slope exists under saturated breaking conditions only if the magnitude of R_{su}^{const} exceeds, roughly, 0.5 (with $c_1 \sim 1$). It is quite possible that under some conditions, only a horizontal slope (or even landward facing slope) would be in equilibrium. This prediction is at odds with existing equilibrium profile models, which have monotonically increasing shapes.

An equilibrium beach profile can be computed for any arbitrary choice of sediment transport formulation so long as it has a linear slope dependence. For the present situation this is simply the solution to a system of ordinary differential equations:

$$\frac{\partial}{\partial x} h = f_1\{h, H_{\text{rms}}\}, \qquad h(x = 0) = h_o$$

$$\frac{\partial}{\partial x} H_{\text{rms}} = f_2\{h, H_{\text{rms}}\}, \qquad H_{\text{rms}}(x = 0) = H_o, \qquad (23)$$

where f_1 describes the equilibrium slope ($\partial h/\partial x = \tan \beta$) and f_2 describes wave height at equilibrium. The subscript "o"
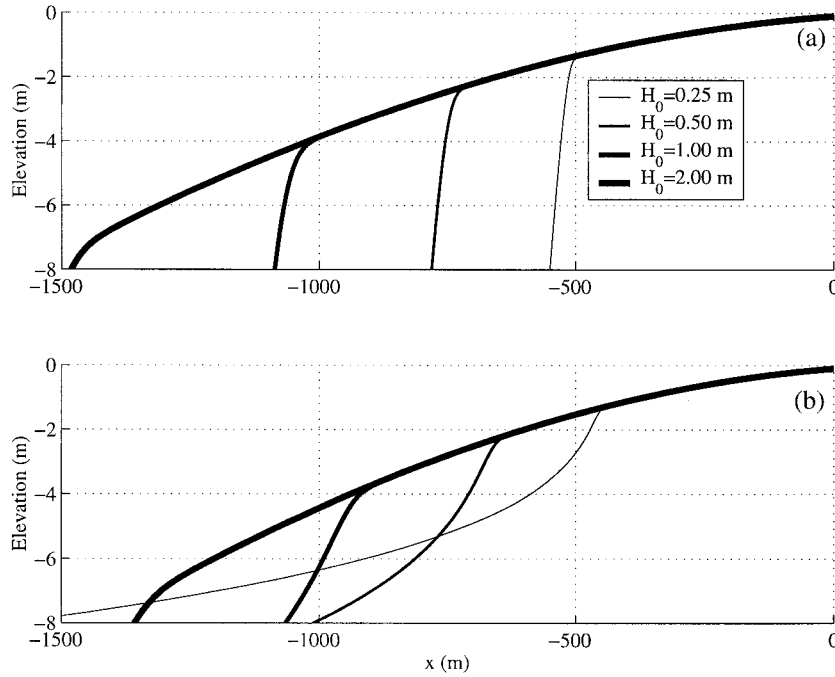
Figure 10. Computed equilibrium profiles for incident, rms wave heights of 0.25 m (thinnest line), 0.5 m, 1 m, and 2 m (thickest line). The two cases considered are (a) equilibrium defined by equation (22a), with $\tan \phi = 0.5$, $c_1 = 1$, and $R_{su}^{\text{other}} = -0.5$ and (b) equilibrium specified by the generalized formula (21c), with $p = 2$, $r_0 = 2.25$, $r_1 = 0.5$, and $y_c = 0.3$. In all cases the wave transformation model (equation (24)) was used with model coefficients $B = 1$, $f_p = 0.1$, and $\gamma_m = 0.4$. The maximum (i.e., saturated) relative wave height in both cases (not shown) was ~0.3. All profiles have been translated so that $x = 0$ corresponds to the shoreline (defined by $h = 0.1$ m).

denotes an initial condition at the seaward boundary. The function f_2 is a wave transformation model. For example, the shallow water approximations to linear wave theory were applied to a model proposed by *Thornton and Guza* [1983], yielding

$$\frac{\partial}{\partial x} H_{\text{rms}} = -\frac{y}{4} \frac{\partial}{\partial x} h + \frac{3}{4} \frac{\sqrt{\pi} B^3}{\gamma_m^2} \frac{f_p \sqrt{h}}{\sqrt{g}}$$
$$\cdot \{[1 + (y^2/\gamma_m^2)]^{-5/2} - 1\} y^4, \qquad (24)$$

where B is an $O(1)$ coefficient that depends on the type of breaking, f_p is the peak frequency of the assumed narrowband sea surface elevation (i.e., wave) spectrum, and γ_m is an $O(1)$ model coefficient describing a "saturation" value of y. The first term in (24) accounts for wave shoaling and the second term accounts for dissipation via breaking.

Figure 10a shows equilibrium profiles that were estimated for several different incident (at the seaward boundary) wave heights, ranging from 0.25 to 2 m. The equilibrium slope was solved via fifth-order Runge-Kutta integration of the system described in (23), where f_1 was given by (22a) and f_2 was given by (24). (Note that the slope is required to compute the wave height gradient in (24). This is supplied by computing f_1 before computing f_2.) The model was initialized at a depth of 8 m. Values for the wave model's coefficients were $B = 1$, $\gamma_m = 0.4$, and $f_p = 0.1$ Hz. The transport model's coefficients were $c_1 = 1$, $R_{su}^{\text{other}} = 0.5$ (large value used to ensure a seaward slope at the shoreline), and $\tan \phi = 0.5$.

The predicted steep slope (equation (22b)) is prominent in the seaward part of profiles when the incident wave height is not saturated. In all cases, the slope approaches a nearly constant value, as y (not shown) reaches a saturation value (~0.3). An interesting feature of these profiles is the wave height dependence of the intersection point between the steep offshore profile and the flat saturation profile. As the wave height increases, the saturation point moves offshore, as does the kink in the profile. Although not necessarily realistic, this feature is suggestive of a "breakpoint" bar (or, perhaps a breakpoint low-tide terrace). The different equilibrium profiles contain different sand volumes. If a natural system is to change from one equilibrium shape to another, deposition or erosion of the subaerial beach or offshore shelf is required. Thus, in cases with limited sand availability (such as a wave tank) it may not be possible for the beach system to attain all equilibrium configurations.

Figure 10b shows examples of the equilibrium profiles calculated using the equilibrium slope specification obtained from (21c), in which $r(y, \tan \beta) = 0$ indicates equilibrium. Values of the coefficients were $p = 2$, $r_0 = 2.25$, $r_1 = 0.5$, and $y_c = 0.3$. These values are consistent with the example in Figure 10a, and they ensure a negative slope (offshore-facing bathymetry) when the relative wave height reaches saturation. The primary difference between the profiles in Figure 10b and those shown in Figure 10a is the concave up shape in the offshore part of the profile, which is more consistent with earlier work [e.g., *Dean*, 1977; *Bowen*, 1980] and more typical of natural beach profiles. In the onshore direction the concave profile intersects a nearly planar profile as a result of wave height saturation. As in Figure 10a, the intersection with the

saturation profile occurs at more seaward locations for larger incident wave heights.

The convex profiles (or portions of profiles) are at odds with the classical "$h = x^{2/3}$" form [*Bowen*, 1980]. However, it is not clear that the profiles shown in Figures 10a and 10b are significantly less realistic than the classical prediction, which includes an infinite slope at the shoreline. Even *Dean*'s [1977] analysis discovered convex profiles (probably ~10% of all cases). Interestingly, the profiles shown in Figures 10a and 10b show a high degree of self-similarity (as do profiles fitting the "$h = ax^m$" family), corresponding to a stretching of the horizontal and vertical axes. Dean's profile analysis would classify the profiles in Figure 10b as either concave or convex, depending on the offshore extent of the measurements.

4.3. Profile Response Time

It is often assumed that beaches asymptotically approach an equilibrium shape, which depends, in part, on the incident wave conditions. This will occur only if the equilibrium profile is, in fact, stable. The stability of the equilibrium profile has not been demonstrated here or in any other nearshore profile model. On the other hand, the presence in nature of apparent instabilities, such as rhythmic sandbars, suggests that not all equilibrium states are stable. Recent stability analyses show that the nearshore profile may be unstable [*Trowbridge*, 1995; *Falques et al.*, 1998]. These stability studies have been restricted to forcing by alongshore currents. A stability analysis of the equilibrium profiles derived here is clearly a logical next step, but this is beyond the scope of this paper.

If, however, we assume that equilibrium profiles are stable, then the relevance of a particular equilibrium state also depends on the response time associated with the approach to that state. A characteristic, morphologic response time that is short relative to the timescale of variations in the forcing indicates that it may be possible to find a profile near equilibrium. If the response time is relatively long, then it may be unlikely to find a profile in equilibrium, although the profile may still strive toward equilibrium.

A response time can be estimated from the sediment conservation equation for cross-shore transport:

$$\frac{\partial h}{\partial t} = \frac{\mu}{\rho_s} \frac{\partial Q}{\partial x}, \qquad (25a)$$

where μ accounts for the porosity of the bed ($\mu = [1 - \nu]^{-1}$, where ν is the bed porosity). A characteristic response time that can be derived from the conservation equation (25a) is

$$\Delta t = T_m = \frac{\rho_s}{\mu} \frac{\Delta h \Delta x}{\Delta Q}, \qquad (25b)$$

where Δh is a typical change in the bed elevation over the time interval Δt (and $\Delta t = T_m$, the morphologic timescale) and Δx is a typical cross-shore length scale. If we assume that the transport vanishes at the shoreline, then ΔQ is a typical transport rate. (This result can be derived more formally by nondimensionalizing equation (25a).)

In order to estimate the morphologic timescale we are free to choose characteristic depth and cross-shore length scales that are appropriate to the nearshore profile. For the depth scale we choose $\Delta h = 0.05 g T^2 (2\pi)^{-1}$, which is the maximum depth where shallow water linear wave theory is appropriate. For a wave period of 10 s, this depth is ~8 m. For the cross-shore length scale we choose $\Delta x = 10 \Delta h / \tan \phi$, which

ensures that slopes satisfy $\tan \beta / \tan \phi \ll 1$. Equation (21b) can be used to estimate the characteristic transport magnitude at a depth of Δh, given a corresponding wave height, $H_{rms} = H_o$. Inserting these choices of scales into (25b), the morphologic timescale is

$$T_m \approx \frac{160 \sqrt{2}}{\mu C_f'} \frac{\rho_s}{\rho_s - \rho} \frac{\rho_s}{\rho} \frac{(\Delta h)^{7/2}}{\sqrt{g}(H_o)^3} \text{ (s).} \qquad (26)$$

We chose typical values for coefficients in (26) (e.g., $\mu = 2$, $C_f' = 10^{-4}$, $\rho_s = 2500$ kg m^{-3}, $\rho = 1000$ kg m^{-3}) and set $\Delta h = 8$ m. Estimated timescales as a function of incident wave height were ~550 years for $H_o = 0.5$ m, 70 years for $H_o = 1$ m, 9 years for $H_o = 2$ m, and 2.5 years for $H_o = 3$ m. These response times are exceedingly long with respect to nearshore hydrodynamic processes. These timescales are upper limits for nearshore evolution, since features with short cross-shore length scales (relative to the profile width that we consider), such as sandbars, will evolve at a faster rate. Interestingly, maximum response times of $O(1 \text{ year})$ are consistent with the estimated timescales of outer bar response observed at Duck, North Carolina (U.S. east coast) [*Plant et al.*, 1999] and along the Dutch coast (H. Hanson et al., Modeling of coastal evolution on yearly decadal timescales, submitted to *Journal of Coastal Research*, 2000).

Even if an order of magnitude uncertainty is introduced into the scaling, the morphologic response times are clearly long compared with the hourly or daily timescale associated with wave height changes. Thus, if nearshore profiles asymptotically approach equilibrium, beach profiles observed in nature must be some sort of a weighted-average of the time-varying equilibria, integrated over time-varying wave conditions. The weights are likely largest for the largest incident wave heights. *Bowen* [1980] made this same point in the first sentence of his paper, but he did not pursue its consequences. Clearly, this situation deserves further attention beyond the scope of this paper.

4.4. Neglected Processes: Relevance of Suspended Load

Our exclusive use of *Bagnold*'s [1963] bed load theory avoided the complication of including and distinguishing between the contributions from bed load and suspended load transport. We note that the form of the transport parameterization for suspended load derived by *Bagnold* [1963] is similar to the bed load form. The suspended load parameterization is, ultimately, more complicated, since the term $\tan \beta / \tan \phi$ is replaced by the varying (on the fast timescale) term U/w_s, where w_s is the sediment fall velocity. We expect, however, that the structure of the generalized transport formulation (equations (21a)–(21c)) is still relevant, since its development was based, in part, on measured suspended load transport. The most significant change induced by an explicit consideration of suspended load transport is most likely seen in the transport magnitude and response time. One of the primary conclusions from previous work [i.e., *Thornton et al.*, 1996; *Gallagher et al.*, 1998] was that predicted magnitudes of suspended load transport exceeded the bed load transport by an order of magnitude under energetic conditions. Thus our response time estimates may be in the range of 2 to 50 months, which are still very long.

4.5. Neglected Processes: Relevance of Grain Size Variation

The effect of grain size, handled explicitly only in suspended load formulations via the fall velocity, is conspicuously missing

from the parameterizations that we have presented (although grain density is included). Grain size effects ought to appear in two places. The first is in the assumed constant parameter c_1 (equation (11)), which is the ratio of concentration standard deviation to mean concentration. A reasonable trend is probably that of c_1 increasing with grain size. Large grains, which have larger fall velocities, will drop out of the water column quickly and give rise to large temporal variability in the sediment load (large c_1). In the limit of very fine grains the grain response time becomes infinitely long, and the sediment load is eventually characterized only by the mean load ($c_1 \rightarrow 0$).

Likewise, the correlation term (i.e., R_{su}^{other} in equation (18b)) is affected by the grain size. Grains with long response times will be advected back and forth many times by the near-bed velocities [*Hay and Bowen*, 1993], and, potentially, the sediment load fluctuations will become uncorrelated to the velocity fluctuations. On the other hand, the movement of coarse grains should be more strongly correlated to the near-bed velocities. Variations of the parameters c_1 and R_{su}^{other} in the manner just described yield predicted equilibrium slopes that are steeper for coarse grains (see (22b) or (22c)) and flatter for fine grain sizes.

5. Conclusions

The approach taken in this paper differed from similar analyses by *Bowen* [1980] and *Bailard* [1981]. We have added to their discussion by considering the morphologic implications associated with strengths and weaknesses of the popular *Bagnold* [1963] model for sediment transport. We isolated the nearshore transport terms that Bagnold's model predicts well (i.e., mean flow) from those that are, apparently, not well predicted (i.e., transport due to correlations between fluctuations in flow and sediment load). In addition, we factored the model into a dimensional transport magnitude and a nondimensional term. The nondimensional term described the relative importance of transport due to undertow, gravity, and correlations between flow and sediment load. Using a bed load formulation for simplicity, the dimensional magnitude term was predicted to increase with wave height cubed, and this term increased inversely with water depth (raised to the 3/2 power). An important conclusion is that the magnitude of transport determines, in part, the response time of nearshore profiles. For typical nearshore environments this response time was estimated to range from 500 years ($H_{\text{rms}} = 0.5$ m) to 2 years ($H_{\text{rms}} = 3$ m). These response times are exceedingly long when compared to the timescale associated with changes in nearshore forcing, which is $O(1 \text{ day})$.

Both the theory and observational data presented here suggested that the relative wave height, $y = H_{\text{rms}}/h$, is the primary variable to include in a parameterization of the relative importance of several cross-shore sediment transport mechanisms. A general form for this parameterization was derived through heuristic arguments based on *Bagnold*'s [1963] theory and on observational data. We conclude that the combined influences of mean flow, flow-sediment correlation, and slope can be well modeled with a polynomial dependence on the relative wave height and linear beach slope dependence.

Simplified parameterizations of nearshore transport were interrogated for the existence and form of equilibrium profiles. Several differences from previously computed equilibrium profiles were noted. First, because the relative wave height saturates in natural surf zones, all equilibrium profiles converged on a relatively flat profile near the shoreline. This differs from the predicted slope steepening encountered in "$x^{2/3}$"-type models. Second, under some situations a seaward sloping equilibrium profile was not found. Interestingly, the nearshore system does not explicitly exclude these conditions. Third, the long profile response times combined with unknown stability of an equilibrium profile make it difficult to assess the practical relevance of equilibrium profiles. If profiles actually evolve toward equilibrium (a stable situation), then the profiles observed in nature must be some sort of weighted average of all possible equilibria. The weighting function probably favors conditions with large wave heights, since these conditions have the shortest response times.

References

Aagaard, T., J. Nielsen, and B. Greenwood, Suspended sediment transport and nearshore bar formation on a shallow intermediate-state beach, *Mar. Geol.*, *148*, 203–225, 1998.

Bagnold, R. A., Mechanics of marine sedimentation, in *The Sea*, vol. 3, *The Earth Beneath the Sea*, edited by M. N. Hill, pp. 507–528, Wiley-Interscience, New York, 1963.

Bailard, J. A., An energetics total load sediment transport model for a plane sloping beach, *J. Geophys. Res.*, *86*, 10,938–10,954, 1981.

Bailard, J. A., and D. L. Inman, An energetics bed load model for a plane sloping beach: Local transport, *J. Geophys. Res.*, *86*, 2035–2043, 1981.

Black, K. P., R. M. Gorman, and G. Symonds, Sediment transport near the break point associated with cross-shore gradients in vertical eddy diffusivity, *Coastal Eng.*, *26*, 153–175, 1995.

Bowen, A. J., Simple models of nearshore sedimentation: Beach profiles and longshore bars, in *The Coastline of Canada*, edited by S. B. McCann, *Pap. Geol. Surv. Can.*, *80-10*, 1–11, 1980.

Cartwright, D. E., and M. S. Longuet-Higgins, The statistical distribution of the maxima of a random function, *Proc. R. Soc. London, Ser. A*, *237*, 212–232, 1956.

Dean, R. G., Equilibrium beach profiles: U.S. Atlantic and Gulf coasts, *Ocean Eng. Tech. Rep.*, *12*, 45 pp., Univ. of Del., Newark, 1977.

Dean, R. G., and R. A. Dalrymple, *Water Wave Mechanics for Engineers and Scientists*, 353 pp., World Sci., River Edge, N. J., 1984.

Deigaard, R., Comparison between a detailed sediment transport model and an energetics based formula, paper presented at Coastal Dynamics Conference, Am. Soc. of Civ. Eng., Plymouth, England, 1998.

Doering, J. C., and A. J. Bowen, Parametrization of orbital velocity asymmetries of shoaling and breaking waves using bispectral analysis, *Coastal Eng.*, *26*, 14–33, 1995.

Elgar, S., and R. T. Guza, Observations of bispectra of shoaling surface gravity waves, *J. Fluid Mech.*, *161*, 425–448, 1985.

Falques, A., A. Montoto, and V. Iranzo, Bed-flow instability of the longshore current, *Cont. Shelf Res.*, *16*, 1927–1964, 1998.

Gallagher, E., R. T. Guza, and S. Elgar, Observations of sandbar evolution on a natural beach, *J. Geophys. Res.*, *103*, 3203–3215, 1998.

Haines, J. W., and A. H. Sallenger Jr., Vertical structure of mean cross-shore currents across a barred surf zone, *J. Geophys. Res.*, *99*, 14,223–14,242, 1994.

Hay, A. E., and A. J. Bowen, Spatially correlated depth changes in the nearshore zone during autumn storms, *J. Geophys. Res.*, *98*, 12,387–12,404, 1993.

Horikawa, K., Coastal sediment processes, *Annu. Rev. Fluid Mech.*, *13*, 9–32, 1981.

Larson, M., and N. C. Kraus, Prediction of cross-shore sediment transport at different spatial and temporal scales, *Mar. Geol.*, *126*, 111–127, 1995.

Lippmann, T. C., and R. A. Holman, The spatial and temporal variability of sandbar morphology, *J. Geophys. Res.*, *95*, 11,575–11,590, 1990.

Masselink, G., and K. P. Black, Magnitude and cross-shore distribution of bed return flow measured on natural beaches, *Coastal Eng.*, *25*, 165–190, 1995.

Phillips, O. M., *The Dynamics of the Upper Ocean*, 336 pp., Cambridge Univ. Press, New York, 1977.

Plant, N. G., R. A. Holman, M. H. Freilich, and W. A. Birkemeier, A simple model for interannual sandbar behavior, *J. Geophys. Res.*, *104*, 15,755–15,776, 1999.

Raubenheimer, B., R. T. Guza, and S. Elgar, Wave transformation across the inner surf zone, *J. Geophys. Res.*, *101*, 25,589–25,597, 1996.

Roelvink, J. A., and I. Brøker, Cross-shore profile models, *Coastal Eng.*, *21*, 163–191, 1993.

Roelvink, J. A., and M. J. F. Stive, Bar-generating cross-shore flow mechanisms on a beach, *J. Geophys. Res.*, *94*, 4785–4800, 1989.

Ruessink, B. G., K. T. Houwman, and P. Hoekstra, The systematic contribution of transporting mechanisms to the cross-shore sediment transport in water depths of 3 to 9 m, *Mar. Geol.*, *152*, 295–324, 1998.

Sallenger, A. H., Jr., and R. A. Holman, Wave energy saturation on a natural beach of variable slope, *J. Geophys. Res.*, *90*, 11,939–11,944, 1985.

Stive, M. J. F., A model for cross-shore sediment transport, paper presented at 20th International Conference on Coastal Engineering, Am. Soc. of Civ. Eng., Taipei, Taiwan, 1986.

Stive, M. J. F., and H. J. de Vriend, Shear stresses and mean flow in shoaling and breaking waves, *Coastal Eng.*, *23*, 594–608, 1994.

Stive, M. J. F., and H. G. Wind, Cross-shore mean flow in the surf zone, *Coastal Eng.*, *10*, 325–340, 1986.

Thornton, E. B., and R. T. Guza, Energy saturation and phase speeds measured on a natural beach, *J. Geophys. Res.*, *87*, 9499–9508, 1982.

Thornton, E. B., and R. T. Guza, Transformation of wave height distribution, *J. Geophys. Res.*, *88*, 5925–5938, 1983.

Thornton, E. B., R. T. Humiston, and W. Birkemeier, Bar/trough generation on a natural beach, *J. Geophys. Res.*, *101*, 12,097–12,110, 1996.

Trowbridge, J. H., A mechanism for the formation and maintenance of shore-oblique sand ridges on storm-dominated shelves, *J. Geophys. Res.*, *100*, 16,071–16,086, 1995.

Werner, B. T., and T. M. Fink, Beach cusps as self-organized patterns, *Science*, *260*, 968–971, 1993.

Wright, L. D., J. D. Boon, S. C. Kim, and J. H. List, Modes of cross-shore sediment transport on the shoreface of the Middle Atlantic Bight, *Mar. Geol.*, *96*, 19–51, 1991.

N. G. Plant, Faculty of Technology and Management, University of Twente, P.O. Box 217, WB-Bldg., NL-7500 AE Enschede, Netherlands. (N.G.Plant@sms.utwente.nl)

B. G. Ruessink, WL/Delft Hydraulics, Marine and Coastal Management, P.O. Box 177, NL-2600 MH Delft, Netherlands. (gerben.ruessink@wldelft.nl)

K. M. Wijnberg, Department of Physical Geography, Utrecht University, P.O. Box 80115, NL-3508 TC Utrecht, Netherlands. (k.wijnberg@geog.uu.nl)